Controlled morphology of Ag nanocolumns by oblique angle deposition: kinetic Monte Carlo simulation

Jingshu Liang (梁景舒), Shuhan Chen (陈书汉), Enyu Lin (林恩宇), and Shaoji Jiang (江绍基)*

State Key Laboratory of Optoelectronic Materials and Technologies, Sun Yat-sen University, Guangzhou 510275, China

**Corresponding author: stsjsj@mail.sysu.edu.cn*

Received November 10, 2012; accepted December 30, 2012; posted online May 10, 2013

Fabrication of Ag or Au nanocolumns by oblique angle deposition (OAD) is now prevalent for their surface enhanced Raman scattering (SERS) property and their biosensor application. However, the size, shape, and the density of nanocolumns are not directed in a desired way. To sufficiently realize the growth process controlled by multiple physical factors like deposition angle (α), substrate temperature (T), and deposition rate (F), we develop a three-dimensional (3D) kinetic Monte Carlo (KMC) model for simulating processes of Ag nanocolumnar growth by oblique angle deposition. The dependences of nanocolumnar morphologies on these factors are analyzed. The mimical results reach a reasonable agreement with the experimental morphologies generated by OAD.

OCIS codes: 310.1860, 310.6805, 310.3840.
doi: 10.3788/COL201311.S10202.

Fabrication of nanostructural thin films by oblique angle deposition (OAD) (also known as glancing angle deposition) is quite prospective in micromechanical systems, catalyst support, optoelectronics, and sensing application[1−7]. Generally, OAD is a physical vapor deposition (PVD) technique in which the vapor atoms are deposited on a substrate at a large deposition angle α ($>70°$) from the surface normal of the substrate[8]. Due to the self-shadowing effect during an OAD, it can generate varied nanostructures and porous thin-film materials associating with unusual physical configurations[9]. Lately, Ag nanocolumn arrays with different lengths fabricated by various vapor deposition angles were discussed systematically on their morphologies, optical reflections, and surface enhanced Raman scatering (SERS) responses in Ref. [8]. However, the nanocolumn arrays are not straightforward to be controlled in a desired way. The dependence of nanocolumnar structures on fabricated factors like the deposition angle, deposition rate, and the substrate temperature in the OAD process should be studied integrallty as to understand the relationship between single atomic interactions and mesoscopic morphologies at large scales.

Before subtle interactions at the atomic level could be precisely controlled by experimental conditions, kinetic Monte Carlo (KMC) simulations have been proven to be a powerful approach to understand growth processes and the mechanism of thin films on a microscopic level, as demonstrated in numerous studies[10−14]. Recently, there are many literatures reporting on nanostructures of metallic thin films by three-dimensional (3D) KMC simulations[15−17]. These mimical studies provided the dependence of asymmetric structures or the surface roughness on the oblique incidence angle, which illustrated the evolution of surface morphologies during OAD processes. And the characteristic length scale of nanorod diameter during growth has been discussed in a (1+1) D KMC model by Zhou *et al.*[18]. However, there are few 3D models proposed that comprehensively analysed multiple experimental parameters.

In our work, we establish a comprehensive 3D KMC model consisting of major parameters in OAD method, such as deposition angle, deposition rate, and substrate temperature. The dependences of nanocolumn density, average diameter, and average separation distance on these parameters are discussed companied with the correspondent simulated morphologies for demonstration. Simultaneously, we compare the results with the self-fabricated and reported experiments.

Our 3D simulation model is performed in an fcc lattice structure of a finite volume $V=L_x\times L_y\times L_z$, with periodic boundary conditions, and $L_x=L_y=512$, whilst L_z can be adjusted according to the surface coverage. As the nearest neighbor distance of Ag in diagonal is 0.288 nm, the lattice period is about 0.204 nm. We assume the substrate as an ideal flat Si surface without defect. The Ag atoms deposited directly onto the first layer above the substrate are allowed to occupy alternate (x, y) locations, as shown in gray in Fig. 1(a). In the second layer, the allowed positions are changed accordingly (see Figs. 1(b) and (c)). The third and fourth layers repeat the symmetry of the first and second layers. In the traditional ballistic deposition (BD) process[19], the atoms are assumed to stick onto the first position where they initially touch the surface and in the downward funneling (DF) process[20,21], the depositing atoms "cascade" when they meet block atoms on the surface until they reach a fourfold hollow site. In this model, atoms follow the ballistic deposition process and the downward funneling process is weak. To be more accurate, the self-shadowing effect is incorporated.

The procedures of possible events are simplified as follows. i) A Ag atom is deposited from a random position at the given height L_z with a selected deposition angle. The deposition rate is L^2F (atoms per second) and the time increment is $t=1/(L^2F)$. L^2 is $L_x\times L_y$ and F is the vertical deposition rate in ML/s.

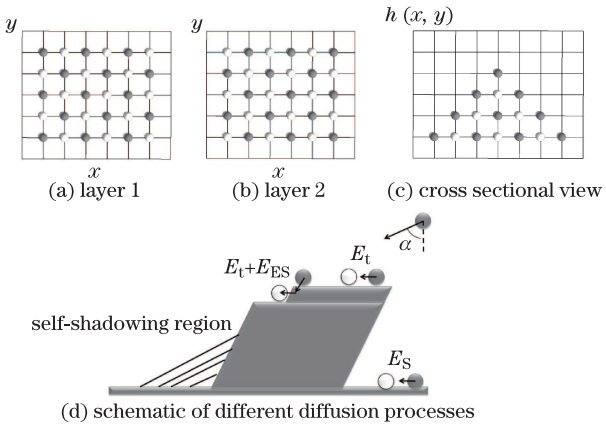

Fig. 1. Model for fcc lattice and diffusion processes. The gray sites indicate the allowed positions for occupation. (a) layer 1; (b) layer 2; (c) cross-sectional view; (d) schemaitc of different diffusion processes.

The deposition angle is a value from the normal of the substrate and the azimuthal angle is zero. The atom will deposit along the orientation of ballistic angle until it meets block atoms. ii) Atoms deposited on the surface diffuse to nucleation or columnar growth depending on their diffusion rates. They can only jump into the nearest-neighbor positions. The diffusion rate D is defined by the Arrhenius rate equation as

$$D_{(ij\rightarrow i'j')} = D_0 \exp(-E/k_{\rm B}T), \qquad (1)$$

where (i, j) is the occupied site, (i', j') is the potential jump site, D_0 is the attempt rate ($\sim 10^{13}$ s^{-1}), $k_{\rm B}$ is the Boltzmann's constant, T is the substrate temperature, and E is the activation energy of an adatom diffusion from (i, j) to (i', j'), which is given by $E=E_{\rm d} + \Delta n E_{\rm b}$ when atoms diffuse on a flat surface. $E_{\rm d}$ is varied in different diffusion surfaces, e.g., $E_{\rm s}$ and $E_{\rm t}$. Δn is the number difference of nearest-neighbor atoms between two sites. $E_{\rm b}$ is the binding energy of a cluster of two atoms. $E_{\rm s}$ is the diffusion barrier on the Si substrate. $E_{\rm t}$ is the terrace diffusion barrier of a single atom on the Ag surface. $E_{\rm ES}$ is extra step-edge barrier named Ehrlich-Schwoebel (ES) diffusion barrier (see Fig. 1(d)). The diffusion probability p_i of an atom hopping to the direction i can be calculated by the formula $p_i=D_i/\sum D_i$. Figure 1(d) illustrates the schematic of three main diffusion processes. The time increment of this step is $\Delta t=(-\ln R)/D$, where R is a random number between 0 and 1. iii) The atom diffuses to the new site specified by ii). Update the diffusion rate for this atom and advance the simulation clock appropriately. The atom will carry on diffusion ii) until the simulation time t is over when it will go to i). We set that an atom can jump to new sites as long as it has more than one nearest vacancy in the same horizontal layer. We assume $E_{\rm s}$=0.5 eV[22], $E_{\rm t}$=0.4 eV, $E_{\rm b}$=0.29 eV, $E_{\rm ES}$=0.07 eV[23,24] and investigate how varying the deposition angle α, the substrate temperature T, and the deposition rate F may affect the morphologies of Ag nanocolumns.

We first present simulations of Ag thin films with different deposition angles at room temperature T=300 K, and at the rate of F=1.5 ML/s ($\sim$ 0.3 nm/s). Figure 2 shows the aerial view of simulation morphologies in varied deposition angles. As well known, the atoms nucleate spontaneously after depositing on the surface and due to self-shadow effect, the high deposition angle leads to the preferential growth of the tallest features on the surface, along with which columnar mounds are shaped and deep grooves are formed resulting in a porous film[25]. Thus isolate nanocolumns separated with voids are formed with the higher thickness. To compare with the simulations, we deposited Ag thin films on Si wafers respectively at high deposition angles of 80° and 85° (see Fig. 3). The deposition was carried out at room temperature (T=300 K) in a high vacuum chamber with a base pressure of 5×10^{-4} Pa. For both experiments, the deposition rate was kept constant at nominal 0.3 nm/s. From Figs. 2 and 3, it is revealed that the simulation morphologies in 80° and 85° are quite analogous with the experimental results.

To characterize the columnar morphologies, we employed the column density (n), average column diameter (d), and average separation distance (λ). Column density and average column diameter are the mean values estimated at the heights of stable growth (coverage$\sim$40 ML). λ is the average distance between two near columns in the dominated direction of shadowing effect, which can be estimated from the height-height correlation function[26]:

$$C(r,s) = \sum \Big[h(x,y) - \overline{h}\Big]\Big[h(x+r,y+s) - \overline{h}\Big], \qquad (2)$$

where $h(x, y)$ is the height of location of (x, y), $h(x+r, y+s)$ is the height at a location of $(x+r, y+s)$, and $\overline{h}$ is the

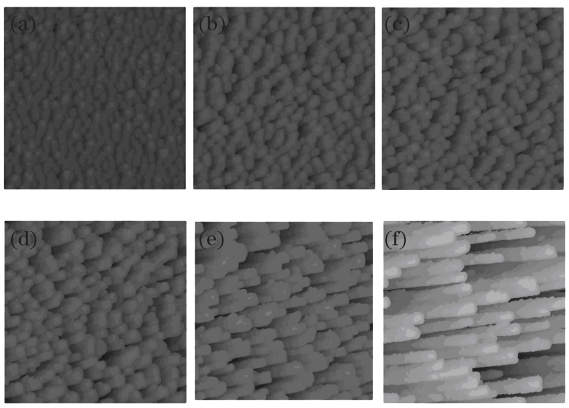

Fig. 2. Aerial view of Ag simulation morphologies at T=300 K and F=1.5 ML/s with deposition angle α: (a) 70°; (b) 78°; (c) 80°; (d) 82°; (e) 85°; (f) 88°.

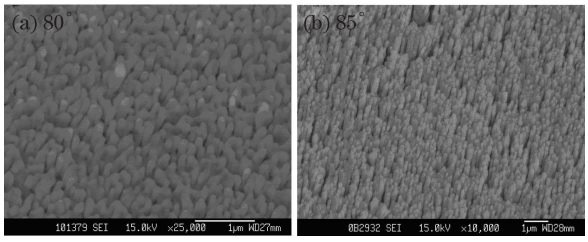

Fig. 3. Scanning electran microscope (SEM) images of Ag at T=300 K and F=0.3 nm/s with deposition angle α: (a) 80° and (b) 85°.

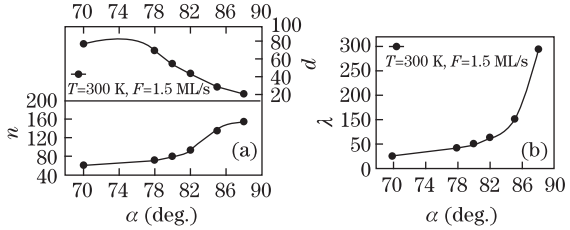

Fig. 4. (a) Average diameter d, column density n, and (b) average separation distance λ as functions of deposition angle α at the deposition rate F=1.5 ML/s and T=300 K. The ordinates of d and λ use lattice units.

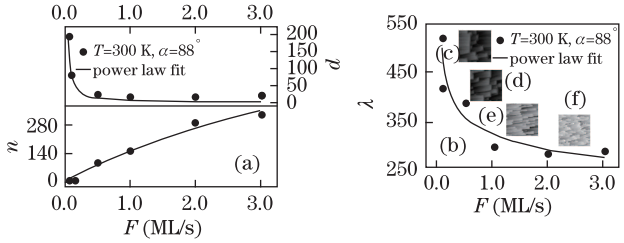

Fig. 5. (a) Average diameter d and column density n, and (b) average separation distance λ as functions of deposition rate F at the deposition angle α=88°, T=300 K, and the related morphologies of simulation at (c) F=0.05 ML/s, (d) F=0.5 ML/s, (e) F=1.0 ML/s, and (f) F=2.0 ML/s. The ordinates of d and λ use lattice units.

average height value. Here, λ was estimated from the normalized $C(r,0)$. In Fig. 4(a), the density and average diameter of Ag columns are described as functions of deposition angle. It can be seen that the diameter decreases as the deposition angle increases whilst the density goes in the opposite trend. This can be explained by the competition between surface diffusion and self-shadowing effect. As α increases, the self-shadowing effect becomes significant with the shadowing length being larger, and the atoms fail in island coalescence for they are restricted to the non-shadowing areas with deficient diffusion in the early stage. Moreover, the growth along with the direction from deposition is strengthened while the lateral growth is weakened in the later stage for the effect of extra step-edge barrier ($E_{\rm ES}$). In this case, more small-size columnar mounds are formed on the surface and the 3D-islanded growth mode is shaped. Simultaneously, the average separation distance ascends dramatically in Fig. 4(b) due to the enlarging voids and vacancies with increasing deposition angle which was explained by the anisotropic growth considering the shadowing effect[17].

From Figs. 2 and 4, one can expect that the average diameter dependence $d(\alpha)$, column density dependence $n(\alpha)$, and average separation distance dependence $\lambda(\alpha)$, are influenced effectively by the deposition angle, in other words, the nanocolumns of Ag could be roughly designed by varying deposition angles, which are as well shown in experiments by Liu *et al.*[8].

As the next phase, we explore the variation of Ag nanocolumns by OAD at an extreme deposition angle α=88° by changing the rates of deposition, which is a major process parameter in PVD technique. Figure 5(a) describes the dependence of the density and average diameter of nanocolumns on deposition rate (F) at a fixed amount of deposited atoms (coverage ~40 ML). The average diameter d decreases enormously with the increase of F till 0.5 ML/s, and then levels off from 0.5 to 3.0 ML/s with the fitted power of –1.15. By contrast, the column density increases smoothly with the increase of F. These two behaviors should originate from the synergy of several elementary processes; on the rather low F (0.05 and 0.1 ML/s), the nearby islands on the surface have sufficient time to merge into larger islands. Simultaneously, there are more atoms on the substrate jumping to the shadowing area, leading to a merged mounded morphology. As the deposition rate increases, the arrival of new atoms on the substrate resulting in nucleation of islands have less time for further coalescence[26] and the shadowing effect prevents partial atoms from adsorbing on the substrate, reducing the coalescence as well. Thus a larger number of small islands are formed on the substrate for later growth. Subsequently more isolated columns with decreasing average diameter d come into formation.

The dependence of $n(F)$ from the scaling law ($n \propto (F/D)^q$) described by Ref. [27] is also shown in Fig. 5. The corresponding exponent value q is estimated to be approximately 0.75, which is larger than 0.55 based on the critical number of bonds adopted in the normal deposition model for 3D geometry[26]. This phenomenon implies that the dependence of 3D columnar mound density from OAD with deposition rate (0.01–3.0 ML/s) is not consistent with the dependence of the island density in normal deposition with slower deposition rate (0.005–0.1 ML/s)[26]. Derived from the scaling law ($n \propto (F/D)^q$), the fitted power law describing the average separation λ at the fixed coverage reads $\lambda \propto (F^{-q/2})$[27]. However, the dependence in Fig. 5(b) is with the power of –0.15, accordingly q is about 0.30, which is different from the asymptotic estimated value of 0.55.

In addition, substrate temperature is another major factor for columns formation in OAD. In practice the average diameter and separation distance of nanocolumns are sensitive to the substrate temperature. We explore the temperature dependence from 235 to 400 K at F=2.5 ML/s (~0.5 nm/s) and α=85° (coverage ~75 ML), the condition of which is relevant to the reported OAD experiments[28]. Figure 6(a) shows that the average diameter ascends whilst the column density descends with the increase of substrate temperature, having the same phenomenon with experiments in 235 and 400 K[28]. This trend originates from accelerating incorporation rate of atomic diffusion on the surface with increasing temperature.

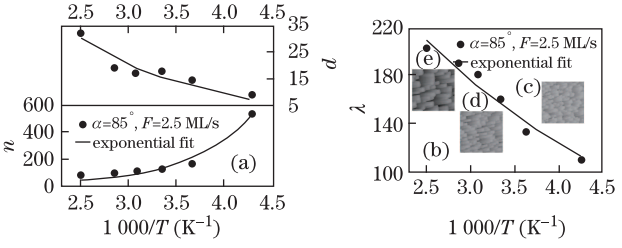

Fig. 6. (a) Average diameter d, column density n, and (b) average separation distance λ as functions of substrate temperature (1 000/T) at the deposition rate F=2.5 ML/s, deposition angle α=85°, and the related morphologies of simulation at (c) T=275, (d) 300, and (e) 400 K. The ordinates of d and λ use lattice units.

Specifically, as the substrate temperature rises, the diffusion rate increases exponentially (see Eq. (1)), the atoms could nucleate into larger islands on the surface in less diffusion time. From the noted Ostwald ripening[29], large islands rnay merge the small ones at elevated temperatures, growing into larger size. Furthermore, the atoms deposited on the top of the preexisting islands consume less time to diffuse to the edge so that they can enlarge the diameter which further strengthens the capability of atom-capture by the columns to grow wider. The exponential dependence of d and n on temperature T^{-1} is also fitted in the graph. The dependence $n(1\,000/T)$ shown in the graph is consistent with $n \propto (e^{q/T})$ in Eq. (1) which can be described as Arrhenius behavior. Figure 6(b) shows the dependence of average separation distance on substrate temperature T^{-1}. As the opposite behavior on deposition flux F, it increases with the accrescent T for the column density is decreased and the vacant space is amplified, which is also explicitly revealed from the mock morphologies at the corresponding conditions in Figs. 6(c), (d), and (e). The fitted exponents for $n(1\,000/T)$, $d(1\,000/T)$, and $\lambda(1\,000/T)$ are 1.47, –0.79, and –0.35, respectively.

From the results above, it implies that by changing deposition rate and substrate temperature, the silver columns can be designed in varied densities, diameters and separation distances during the OAD processes. Though the scaling laws show a reasonable approximation for deposition processes with a fixed coverage, experimentally, the fabrication of nanocolumns in oblique angle deposition may depend on multiple various factors, which cannot be all figured out by simple analytical dependencies.

In conclusion, we present a simple but systematic 3D KMC simulation model for thin film growth of Ag nanocolumns by OAD, which Ag validated by comparison with experiments. Employing the model, we explore the capabilities to control the morphologies of Ag nanocolumns by varying the major OAD process conditions, such as the deposition angle, deposition rate, and the substrate temperature, which are applicable to the realistic deposition experiments. Generally, enlarging the deposition angle leads to enhance the average separation distance and the density of columns, increasing the deposition rate results in dense columns and less separation distance while ascending the substrate temperature produces larger nanocolumns and more vacant separation distance between columns. Furthermore, we fit the dependence of average diameter, column density, and average separation distance on deposition rate and substrate temperature respectively, resulting in reasonable scaling laws. With the analogous mimical morphologies and simple scaling laws, we expect that this model will facilitate the OAD process design of Ag nanocolumns. In spite of this, the scaling laws of metallic nanocolumns in OAD need more precise proof and complement in practice. Moreover, a more accurate model including the diffusion of dimers, substrate defects, interstitials diffusion, and mismatched substrate lattices which are contributed to the columnar growth in reality should be established in the future.

This work was supported by the National Natural Science Foundation of China under Grant Nos. 61275159, 60977042, and 11074311.

References

1. A. T. Wu, M. J. Brett, and D. J. Broer, Sens. Mater. **13,** 399 (2001).
2. S. R. Kennedy and M. J. Brett, Nano Lett. **2,** 59 (2002).
3. K. D. Harris, J. R. McBride, K. E. Nietering, and M. J. Brett, Sens. Mater. **13,** 225 (2001).
4. Y. P. Zhao, D. X. Ye, P. I. Wang, G.-C. Wang, and T.-M. Lu, Int. J. Nanosci. **1,** 87 (2002).
5. M. W. Seto, B. Dick, and M. J. Brett, J. Micromech. Microeng. **11,** 582 (2001).
6. M. Malac and R. F. Egerton, J. Vac. Sci. Technol. A **19,** 158 (2001).
7. Y.-P. Zhao, D.-X. Ye, G.-C. Wang, and T.-M. Lu, Nano Lett. **2,** 351 (2002).
8. Y.-J. Liu, H. Y. Chu, and Y.-P. Zhao, J. Phys. Chem. C **114,** 8176 (2010).
9. M. J. Brett and M. M. Hawkeye, Science **319,** 1192 (2008).
10. L. Nurminen, A. Kuronen, and K. Kaski, Phys. Rev. B **63,** 035407 (2000).
11. J. B. Adams, Z. Y. Wang, and Y. Li, Thin Solid Film **365,** 201 (2000).
12. C.-L. Li and C.-K. Hu, Appl. Phys. Lett. **96,** 093101 (2010).
13. G. L. Yu, J. G. Zhu, W. Lu, and D. Q. Xiao, Mater. Des. **27,** 710 (2006).
14. S. M. H. Haghighat and A. K. Taheri, Mater. Des. **28,** 2533 (2007).
15. X. Tan, Y. C. Zhou, and X. J. Zheng, Surf. Sci. **588,** 175 (2005).
16. L. A. Zepeda-Ruiz, E. Chason, G. H. Gilmer, Y. M. Wang, H. W. Xu, A. Nikroo, and A. V. Hamza, Appl. Phys. Lett. **95,** 151910 (2009).
17. Y. Shim and J. G. Amar, Phys. Rev. Lett. **98,** 046103 (2007).
18. L. G. Zhou and H. Huang, Phys. Rev. Lett. **101,** 266102 (2008).
19. P. Meakin, P. Ramanlal, L. M. Sander, and R. C. Ball, Phys. Rev. A **34,** 5091 (1986).
20. J. W. Evans, D. E. Sanders, P. A. Thiel, and A. E. DePristo, Phys. Rev. B **41,** R5410 (1990).
21. J. W. Evans, Phys, Rev. B **43,** 3897 (1991).
22. K. Kong, H. W. Yeom, D. Ahn, H. Yi, and B. D. Yu, Phys. Rev. B **67,** 235328 (2003).
23. P. A. Thiel and J. W. Evans, J. Phys. Chem. B **108,** 14428 (2004).
24. K. J. Caspersen, A. R. Layson, C. R. Stoldt, V. Fournee, P. A. Thiel, and J. W. Evans, Phys. Rev. B **65,** 193407 (2002).
25. L. A. Zepeda-Ruiz, E. Chason, G. H. Gilmer, Y. Wang, H. Xu, A. Nikroo, and A. V. Hamza, Appl. Phys. Lett. **95,** 151910 (2009).
26. A. K. Bhuiyan, S. K. Dew, and M. Stepanova, J. Phys. Chem. C **115,** 19557 (2011).
27. J. A. Venables, Surf. Sci. **299,** 798 (1994).
28. Q. Zhou, Z. C. Li, Y. Yang, and Z. J. Zhang, J. Phys. D: Appl. Phys. **41,** 152007 (2008).
29. H. G. Yang and H. C. Zeng, J. Phys. Chem. B **108,** 3492 (2004).